The prototypic class Ia ribonucleotide reductase from Escherichia coli: still surprising after all these years

The prototypic class Ia ribonucleotide reductase from *Escherichia coli*: still surprising after all these years

Edward J. Brignole[*,†,1], Nozomi Ando[*,†,1], Christina M. Zimanyi[†] and Catherine L. Drennan[*,†,‡,2]
[*]Howard Hughes Medical Institute and [†]Department of Chemistry and [‡]Department of Biology, Massachusetts Institute of Technology, Cambridge, MA 02139, U.S.A.

Key words:
allostery, oligomerization, protein-protein interactions, conformational equilibrium, feedback regulation, nucleotide biosynthesis

Abbreviations used:
RNR, ribonucleotide reductase
NDP, ribonucleoside 5'-diphosphate
PCET, proton-coupled electron transfer
PELDOR, pulsed electron-electron double resonance
AUC, analytical ultracentrifugation
SAXS, small-angle X-ray scattering
EM, electron microscopy

[1]These authors contributed equally to the work.

[2]To whom correspondence should be addressed (email cdrennan@mit.edu)

Abstract
Ribonucleotide reductases (RNRs) are key players in nucleic acid metabolism, converting ribonucleotides to deoxyribonucleotides. As such, they maintain the intracellular balance of deoxyribonucleotides to ensure the fidelity of DNA replication and repair. The best-studied RNR is the class Ia enzyme from *Escherichia coli*, which employs two subunits to catalyze its radical-based reaction: β_2 houses the diferric-tyrosyl radical cofactor and α_2 contains the active site. Recent applications of biophysical methods to the study of this RNR have revealed the importance of oligomeric state to overall enzyme activity and suggest unprecedented subunit configurations are in play. Although it has been five decades since the isolation of nucleotide reductase activity in extracts of *E. coli*, this prototypic RNR continues to surprise us after all these years.

Introduction

In all organisms, propagation of genetic material from one generation to the next requires DNA replication. The accuracy of the genetic copy and the repair of mistakes depend on balanced levels of ribonucleotides and deoxyribonucleotides [1-3]. One remarkable enzyme, ribonucleotide reductase (RNR), converts all four ribonucleotides into deoxyribonucleotide precursors for DNA synthesis and repair. Because of its crucial metabolic role in dividing cells, RNR has an important place in medicine as the target of several clinically used cancer drugs, such as gemcitabine and clofarabine [4, 5].

All RNRs employ a radical-based mechanism for catalysis and are classified by the metallocofactor used to generate an essential thiyl radical within a structurally conserved α/β-barrel substrate-binding domain [6-8]. Once the thiyl radical is generated, nucleotide reduction proceeds through a conserved mechanism (Fig. 1) [9, 10]. Eukaryotes and some aerobic prokaryotes employ class Ia RNRs, which utilize a diferric-tyrosyl radical cofactor for the reduction of ribonucleoside disphosphates (NDPs) [11]. In addition to having a complex catalytic mechanism, RNRs employ sophisticated allostery to maintain the appropriate nucleotide balance in the cell (recently summarized in [12]). Here, we focus on the *E. coli* enzyme, which has long served as the prototype for class Ia RNRs, and review how structural biology techniques have illuminated its catalytic mechanism and allosteric regulation.

Surprising structures of domains

In class Ia RNRs, thiyl radical generation in the active site is achieved by intermolecular interactions between two separate proteins: the nucleotide-binding protein encoded by the gene *nrdA* and the radical-generating protein encoded by the gene *nrdB* [13]. For the canonical class Ia enzymes, including the prototypic *E. coli* enzyme, the NrdA and NrdB proteins form homodimers called α_2 and β_2, respectively (Fig. 2). A diferric-tyrosyl radical cofactor is assembled in β_2 at Tyr122 in the presence of molecular oxygen, Fe(II), and an electron source [14-16]. For each turnover, the formation of the active holocomplex triggers long-range proton-coupled electron transfer (PCET), reducing the Tyr122 radical in β_2 and oxidizing Cys439 in the active site of α_2 to form the essential thiyl radical [17].

A number of crystal structures of the individual α_2 and β_2 subunits have been determined for the *E. coli* enzyme. The β_2 structure is often described as a heart-shaped dimer (Fig. 2B) [18]. One surprise from the β_2 structure was that the tyrosine residue (Tyr122) that harbors the tyrosyl radical is buried in the center of each β protomer, adjacent to its diiron center, 10 Å from the surface. This observation suggested the need for the radical to transfer through other residues to reach the surface of β_2 en route to the substrate-binding site of α_2. Such a long-range electron transfer was unprecedented at the time it was proposed [8] but is now well supported by experimental evidence [19-21]. Another finding from the β_2 structure was that the 32 C-terminal residues were not observed due to their thermal lability (Fig. 2B, dotted curves) [18]. Earlier studies demonstrated that C-terminal residues of β_2 were critical for its interaction with α_2 [22, 23]. Just upstream from this C-terminal sequence within the unstructured tail is the absolutely conserved Tyr356 that subsequent studies have shown to be part of the radical relay between the RNR subunits [19, 24, 25].

Shortly after the first β_2 structure, an equally surprising α_2 structure was reported [8] (Fig. 2A). The α_2 structure was the first example of the 10-stranded α/β barrel that is now known to be characteristic of all three classes of RNR [6, 7]. Cys439, the residue that harbors the catalytic thiyl radical, was located at the tip of a "finger loop" poking into the middle of the barrel. This

residue was located adjacent to the absolutely conserved Cys225 and Cys462 residues that provide the reducing equivalents for nucleotide reduction (Fig. 1, 2A) [10]. In this structure Cys225 and Cys462 were observed in their oxidized state as a disulfide bonded cystine. Furthermore, the positions of Tyr730 and Tyr731 relative to Cys439 implicated their involvement in PCET from β_2 to α_2 (Fig. 2A). Like β_2, α_2 has an unstructured C-terminal tail that also contains residues involved in catalysis. Two cysteine residues, Cys754 and Cys759, in the flexible α_2 tail are responsible for accessing the active site to reduce the Cys225-Cys462 disulfide at the end of each catalytic cycle (Fig. 1) [10, 26]. Additionally, the structure of α_2 was obtained by co-crystallization with a 20-residue C-terminal peptide of β_2, revealing an important determinant of the α_2-β_2 interaction [23], but again density for Tyr356 was not observed (Fig. 2A, orange ribbons).

Early experiments with the *E. coli* class Ia enzyme revealed that deoxynucleotide effectors and ATP are responsible for regulating substrate specificity as well as overall enzyme activity [12, 27]. Nucleotide-binding sites in *E. coli* α_2 were located by further crystallographic work [28]. Crystals of α_2 co-crystallized or soaked with the effector, dTTP, yielded information about the allosteric site known as the "specificity site". The resultant structures showed dTTP bound at either end of a four-helix bundle formed at the α_2 dimer interface, approximately 15 Å from the active site (Fig. 2A) [28]. The specificity effector bound at this site appears to communicate with the active site by ordering the conformation of flexible loops, including one termed "loop 2", which is adjacent to the active site [28]. Consistent with the ancient origin of RNR, this specificity-regulating feature is conserved in the other RNR classes [7, 12, 29, 30]. However, although GDP reduction is promoted by dTTP, structures determined from crystals soaked with this substrate/effector pair showed low substrate occupancy, even for a Cys292-Ala mutant with enhanced GDP affinity and using dithiothreitol to reduce the active site disulfide [28]. Thus, we do not yet have a molecular level picture of how effectors at this site determine substrate specificity for the *E. coli* enzyme. The α_2 subunit also has a third nucleotide-binding site that accepts ATP to activate or dATP to inhibit overall catalytic activity (Fig. 2A) [12]. This "activity site" was located in the same study using crystals soaked with the substrate, CDP, and the ATP analog, AMP-PNP [28]. In the resulting structure, AMP-PNP was observed at the N-terminus of the protein in the so-called "cone domain", a four-helix bundle that is found across class Ia enzymes [31]. However, it was not evident from this structure how binding of ATP or dATP to the cone domain would communicate a signal to the distant active site over approximately 40 Å. In addition, although ATP is also the specificity effector for CDP, AMP-PNP was only weakly present at the specificity site, and the substrate molecule was not observed in the active site [28].

Insight into the structural components of an active RNR complex

To afford enzymatic turnover, α_2 and β_2 must interact allowing for radical transfer to the active site. However, structural data describing the active complex of *E. coli* class Ia RNR has been challenging to obtain. Seminal studies on this RNR led to the proposal that active enzyme exists as an $\alpha_2\beta_2$ complex [32, 33]. Using sucrose gradient centrifugation, mixtures of α_2 and β_2 in the absence of nucleotides or in the presence of ATP or dTTP were shown to sediment at around 8.8-9.7 S with an apparent 1:1 subunit stoichiometry [33]. In a later study, analytical ultracentrifugation (AUC) was repeated in the absence of sucrose, which can perturb protein-protein interactions, to show again that an equimolar mixture of α_2 and β_2 sedimented at around

10 S with an apparent molecular weight that is consistent with an $\alpha_2\beta_2$ oligomerization state [32]. Together, these studies suggested that the active quaternary structure is an $\alpha_2\beta_2$ complex.

The determination of the individual α_2 and β_2 structures that followed two decades later showed that the two dimeric proteins were complementary in shape and therefore could plausibly form an active $\alpha_2\beta_2$ complex [8, 18]. When the two structures are docked along their 2-fold symmetry axes, the lobes of the heart-shaped β_2 neatly fit in the concave pockets containing the active sites of α_2 (Fig. 3A) [8]. Importantly, the subunit arrangement in this model places residues that are important for radical transfer in close proximity across the α_2-β_2 interface. In the proposed PCET pathway, radical propagation occurs along conserved aromatic residues: from Tyr122→Trp48→Tyr356 in β_2 to Tyr731→Tyr730→Cys439 in α_2 [17]. These residues form a conduit in the $\alpha_2\beta_2$ docking model, with the surface-exposed Trp48 of β_2 within ~23 Å from Tyr731 of α_2, a reasonable distance for PCET if bridged by Tyr356 on the flexible C-terminal tail of β_2 (Fig. 3A). Site-directed mutation of each of these conserved residues eliminated activity to background levels, consistent with their proposed involvement in the PCET pathway [25, 34-36]. More recently, incorporation of unnatural amino acids that act as radical traps at Tyr356, Tyr731, and Tyr730 has permitted the direct demonstration of redox-coupling between these residues [20, 21, 24]. Furthermore, these mutants enabled measurements of Tyr122-Tyr731 and Tyr122-Tyr730 distances by pulsed electron-electron double resonance (PELDOR) spectroscopy [19, 37]. These measured distances were consistent with those predicted by the $\alpha_2\beta_2$ docking model and thus provided the first experimental support for the subunit arrangement in this model.

Recently, AUC studies of class Ia RNR were reinitiated, and showed that the sedimentation value of equimolar mixtures of α_2 and β_2 in the presence of activating allosteric effectors is highly dependent on protein concentration and able to exceed 11.5 S, the theoretical value for the globular $\alpha_2\beta_2$ complex predicted by the docking model [38]. This concentration-dependent behavior indicated that the active complex is embedded in an equilibrium mixture and able to interconvert not only with dissociated species but also with a higher order complex, offering an explanation for the elusiveness of the active complex to crystallographic techniques that benefit from homogeneous samples.

Small-angle X-ray scattering (SAXS) was used to extract structural information for the active complex from the equilibrium mixture and provide the first structural evidence that the active complex is well described by the $\alpha_2\beta_2$ docking model [38]. Under assay conditions where α_2 and β_2 should be 97% in an active conformation, the resultant shape reconstruction shows a globular molecule, consistent with the close subunit arrangement in the docking model (Fig. 3B, left). The excess density seen in this shape reconstruction was shown to be due to the presence of a small population of the higher order complex interconverting with the predominant $\alpha_2\beta_2$ complex [38]. When data are subjected to a global analysis, the contribution of the higher order complex can be quantified and therefore subtracted from the SAXS data, yielding a shape reconstruction that represents the active complex on its own (Fig. 3A, right).

First structures of the dATP-inhibited state of *E. coli* RNR complex

In addition to the quest for a structure of active *E. coli* class Ia RNR, a structure depicting both α_2 and β_2 in a dATP-inhibited state has been long sought. Early ultracentrifugation studies provided the first evidence that allosteric inhibition of class Ia RNR by dATP is coupled with higher order oligomerization [32, 33]. Recently, the role of oligomerization in the activity regulation of the *E. coli* enzyme was revisited with multiple biophysical techniques [38, 39]. These studies have

converged on a consistent picture involving the formation of an $\alpha_4\beta_4$ complex under dATP inhibition [38, 39] and have led to the elucidation of the first structures of this complex [38].

A number of low-resolution techniques were used to determine the oligomerization state of the dATP-inhibited *E. coli* enzyme. In a gas-phase electrophoretic mobility macromolecule analysis (GEMMA) study, a heavy complex was observed in the presence of inhibiting dATP concentrations with an electrophoretic mobility diameter that is consistent with a molecular weight of 510 kDa [39]. This heavy complex was shown to have an $\alpha_4\beta_4$ subunit stoichiometry with the use of a β construct tagged with the 57-kDa NusA protein in order to distinguish the α-monomer from the similarly sized β_2 [39]. More recently, AUC and SAXS were used to confirm the molecular weight and subunit composition of the dATP-inhibited $\alpha_4\beta_4$ complex and further show the stability of this species in solution over a wide range of RNR concentrations [38]. Furthermore, both the sedimentation rate and the power-law dependence observed in the X-ray scattering indicated that this $\alpha_4\beta_4$ complex is highly non-globular in shape [38].

The first structures of the dATP-inhibited $\alpha_4\beta_4$ were determined by single particle electron microscopy (EM) and X-ray crystallography, revealing a ring-shaped complex with an alternating arrangement of α_2 and β_2 subunits (Fig. 4) [38]. In this study, the $\alpha_4\beta_4$ rings were the dominant species observed in EM images of α_2 and β_2 mixtures under dATP inhibition. A three-dimensional EM reconstruction of this species generated at 23-Å resolution was fit with crystal structures of the individual subunits, yielding a pseudo-atomic model. This pseudo-atomic model was nearly superimposable with a 5.7-Å resolution crystal structure of the $\alpha_4\beta_4$ ring obtained by co-crystallizing α_2 and β_2 with dATP, demonstrating the structural stability of this complex even at the dilute protein concentrations used for EM. Furthermore, the theoretical sedimentation rate and X-ray scattering profile predicted from these structures closely matched experimental AUC and SAXS data, indicating that this $\alpha_4\beta_4$ ring exists in solution at physiologically relevant RNR and dATP concentrations [38]. Moreover, a low-resolution molecular envelope obtained from SAXS resembled the both EM model and crystal structure, showing consistency among the three structural techniques [38].

The structures obtained from this study provide insight into how dATP inhibits the prototypic class Ia enzyme from *E. coli* [38]. The ring is formed by contacts made by β_2 to the α_2 N-terminal cone domains housing the activity sites, such that Trp48 in β_2 and Tyr731 in α_2 face a large solvent-exposed hole (Fig. 4). In the crystal structure, dATP is observed in both the activity and specificity sites in the crystal structure. Consistent with this result, the $\alpha_4\beta_4$ complex was shown by SAXS to maximally form at above 4 molar equivalents of dATP per α_2. Additionally, in the crystal structure, C-terminal residues of β_2 were observed at the peptide-binding site of each α-protomer (Fig. 4). However, there is broken electron density between Leu339 and Ser363 that again prevented visualization of the elusive Tyr356. While nucleotide reduction by the class Ia RNR depends on the juxtaposition of α_2 and β_2 to permit the round-trip radical relay from Tyr122 to Cys439, the distance between the closest visible residues in the PCET pathway (Trp48 in β_2 and Tyr731 in α_2) in the $\alpha_4\beta_4$ complex is ~55 Å (Fig. 4). The ~55 Å distance is too long to accommodate the radical transfer even with a bridging Tyr356 and would require the implausible scenario of radical transfer through bulk solvent [40]. Together, these structures suggest that the dATP-binding at the activity sites inhibits RNR by stabilizing an open subunit arrangement of α_2 and β_2 that physically separates the PCET residues, preventing radical transfer.

Model for allosteric regulation

These recent developments in the structural characterization of *E. coli* class Ia RNR have provided a new understanding of allosteric activity regulation for this protein. We now know that the prototypic class Ia RNR from *E. coli* exists in at least three states that are supported by direct structural observation: the dissociated α_2 and β_2 subunits [8, 18], the active $\alpha_2\beta_2$ complex [38], and the inhibited $\alpha_4\beta_4$ complex [38]. Furthermore, it was shown by AUC and SAXS that in the presence of activating effectors or in the absence of any effectors, the *E. coli* enzyme exists as an equilibrium mixture of α_2, β_2, $\alpha_2\beta_2$, and $\alpha_4\beta_4$, whose distributions are sensitive to protein concentration. In contrast, dATP is uniquely able to push the equilibrium towards a single $\alpha_4\beta_4$ state [38]. From these data a three-state model emerges for the allosteric regulation of overall activity in *E. coli* class Ia RNR. Here active $\alpha_2\beta_2$ complex is an intermediate between the dissociated state and the inhibited $\alpha_4\beta_4$ complex (Fig. 5). While increases in protein or dATP levels shift the equilibrium to the right, according to this model, ATP may upregulate the *E. coli* enzyme by competing with dATP for binding at the activity site and shifting the equilibrium away from the inhibited $\alpha_4\beta_4$ complex. Thus, in the cell, RNR may act like a molecular thermostat that senses the balance between ribonucleotide and deoxyribonucleotide pools by the competitive binding of ATP and dATP for the activity site, which in turn modulates the equilibrium between the active $\alpha_2\beta_2$ and inhibited $\alpha_4\beta_4$ complexes.

In *E. coli*, the *nrdA* and *nrdB* genes are on the same operon and are thus co-expressed [13]. The ability to form $\alpha_4\beta_4$ provides the *E. coli* enzyme with a clever mechanism for regulating activity by keeping its subunits together but in a nonproductive arrangement. The structure of the dATP-inhibited $\alpha_4\beta_4$ suggests that interconversion between these states can readily occur. Each contact at the cone domains containing the activity site buries a ~500 $Å^2$ interface involving only a handful of residues from each subunit. In addition to the contacts involving the activity site, interconversion between $\alpha_2\beta_2$ and $\alpha_4\beta_4$ maybe facilitated by the flexible C-terminal tails of β_2. While both C-terminal tails from a single β_2 may be interacting with a single α_2 in the compact active complex, the crystal structure of the $\alpha_4\beta_4$ complex suggests that the C-terminal tails of a single β_2 may be used to recruit two α_2 subunits. The C-terminal tails may allow α_2 and β_2 to remain flexibly linked in order to rapidly switch from a closed to open conformation and vice versa (Fig. 5).

Future directions

Recent advances bring clarity to the early observations that suggested a link between activity regulation and oligomerization in the class Ia RNR of *E. coli*, yet many important problems remain to be solved [38]. High-resolution structures of α_2 both alone and in complex with β_2 in the presence and absence of the activity site effectors, ATP and dATP, are needed to understand at an atomic level the conformational changes in the activity site. In existing *E. coli* α_2 crystal structures, the cone domains containing the activity sites make lattice packing interactions [8, 28], and therefore new crystallization conditions might be required to unambiguously resolve details of effector-induced rearrangements at the cone domain. While structures of α_2 with specificity effector/substrate pairs have been determined for the yeast class Ia RNR [41], the effect of β_2 in an active $\alpha_2\beta_2$ complex on specificity regulation is not yet known for any class Ia enzyme. Furthermore, species-specific differences between the sequences at the specificity site [41, 42] suggest that a more complete model of specificity regulation in the *E. coli* enzyme will require structures with full occupancy substrate/effector pairs.

Eukaryotic class Ia RNRs subscribe to a qualitatively similar regime of activity and specificity regulation as their prokaryotic homologs [43-45]. However, the relationship between

oligomerization and allostery in the eukaryotic class Ia RNRs is not as well defined as in prokaryotes. In contrast to the *E. coli* homolog that requires both subunits to form the inhibited oligomer [33, 38, 39], the eukaryotic α_2 alone can oligomerize under both ATP-activation and dATP-inhibition [42, 43, 46-48]. Recently, the dATP-stabilized complex from yeast was shown to be a hexameric ring of α subunits with the cone domains again forming intersubunit contacts [42]. Without structural information on the active form of eukaryotic class Ia RNRs, however, it is not yet clear why this dATP-induced α_6 arrangement would be inactive. A comparison between the structures of the dATP- and ATP-induced complexes is needed to understand its unique twist to this developing saga of allosteric regulation. Excitingly, differences in the allosteric regulation of eukaryotic and prokaryotic class Ia RNRs may permit the future design of allosteric inhibitors that target specific RNRs, such as the RNRs of pathogens.

Finally, little is known about the interaction between the α_2 and β_2 subunits in the active complex. The long-sought atomic resolution structure of the active $\alpha_2\beta_2$ would reveal the positions of residues involved in PCET and might provide critical insight into the conformational changes that trigger radical transmission. In particular, the position of Tyr356 on the C-terminal tail of β_2 has not yet been visualized in any of the available structures. Moreover, mounting evidence establishes that only one of the two active sites in RNR is engaged in radical transfer and substrate reduction at a time [37, 49-52]. Such half-sites reactivity suggests asymmetry in the interaction between α_2 and β_2 that might finally be explained by a high-resolution structure of the active complex. Presumably, the difficulty in obtaining a high-resolution structure of an active complex derives from the dynamic properties of the subunit interactions, the full nature of which was recently emphasized in AUC and SAXS studies [38].

Although five decades have passed since the discovery of the prototypic class Ia enzyme from *E. coli*, RNRs continue to amaze us with their elaborate modes of allosteric regulation, dramatic conformational changes, and complex radical transfer pathways. In the latest chapter, two decades since the first structures of *E. coli* α_2 and β_2 were determined [8, 18], we now have the first low-resolution reconstruction of an active $\alpha_2\beta_2$ complex and the first X-ray and EM structures of the dATP-inhibited $\alpha_4\beta_4$ complex for the *E. coli* enzyme [38]. These studies reveal the transient nature of the active complex and an unanticipated ring-shaped structure for the dATP-inhibited complex, adding a new twist to the RNR story and promising more surprises to come in the future.

Acknowledgements
We are indebted to our collaborators for their contributions to much of the science we describe, Michael A. Funk, Kenichi Yokoyama, JoAnne Stubbe, and Francisco J. Asturias. We would also like to thank JoAnne Stubbe, Joseph A. Cotruvo, and Patrick G. Holder for helpful discussion in preparing this mini review.

Funding
This work was supported by the National Institutes of Health [T32GM08334 (C.M.Z), F32GM904862 (N.A.), K99GM100008 (N.A.), F32DK080622 (E.J.B.), and P30-ES002109 (C.L.D.)]. C.L.D. is a Howard Hughes Medical Institute Investigator.

References

1 Gon, S., Napolitano, R., Rocha, W., Coulon, S. and Fuchs, R. P. (2011) Increase in dNTP pool size during the DNA damage response plays a key role in spontaneous and induced-mutagenesis in *Escherichia coli*. Proc. Natl. Acad. Sci. U. S. A. **108**, 19311-19316

2 Kumar, D., Abdulovic, A. L., Viberg, J., Nilsson, A. K., Kunkel, T. A. and Chabes, A. (2011) Mechanisms of mutagenesis in vivo due to imbalanced dNTP pools. Nucleic Acids Res. **39**, 1360-1371

3 Wheeler, L. J., Rajagopal, I. and Mathews, C. K. (2005) Stimulation of mutagenesis by proportional deoxyribonucleoside triphosphate accumulation in *Escherichia coli*. DNA Repair. **4**, 1450-1456

4 Bonate, P. L., Arthaud, L., Cantrell, W. R., Jr., Stephenson, K., Secrist, J. A., 3rd and Weitman, S. (2006) Discovery and development of clofarabine: a nucleoside analogue for treating cancer. Nat. Rev. Drug Discov. **5**, 855-863

5 Hertel, L. W., Boder, G. B., Kroin, J. S., Rinzel, S. M., Poore, G. A., Todd, G. C. and Grindey, G. B. (1990) Evaluation of the antitumor activity of gemcitabine (2',2'-difluoro-2'-deoxycytidine). Cancer Res. **50**, 4417-4422

6 Logan, D. T., Andersson, J., Sjöberg, B. M. and Nordlund, P. (1999) A glycyl radical site in the crystal structure of a class III ribonucleotide reductase. Science. **283**, 1499-1504

7 Sintchak, M. D., Arjara, G., Kellogg, B. A., Stubbe, J. and Drennan, C. L. (2002) The crystal structure of class II ribonucleotide reductase reveals how an allosterically regulated monomer mimics a dimer. Nat. Struct. Biol. **9**, 293-300

8 Uhlin, U. and Eklund, H. (1994) Structure of ribonucleotide reductase protein R1. Nature. **370**, 533-539

9 Licht, S., Gerfen, G. J. and Stubbe, J. (1996) Thiyl radicals in ribonucleotide reductases. Science. **271**, 477-481

10 Mao, S. S., Holler, T. P., Yu, G. X., Bollinger, J. M., Jr., Booker, S., Johnston, M. I. and Stubbe, J. (1992) A model for the role of multiple cysteine residues involved in ribonucleotide reduction: amazing and still confusing. Biochemistry. **31**, 9733-9743

11 Cotruvo, J. A. and Stubbe, J. (2011) Class I ribonucleotide reductases: metallocofactor assembly and repair in vitro and in vivo. Annu. Rev. Biochem. **80**, 733-767

12 Hofer, A., Crona, M., Logan, D. T. and Sjöberg, B. M. (2012) DNA building blocks: keeping control of manufacture. Crit. Rev. Biochem. Mol. Biol. **47**, 50-63

13 Hanke, P. D. and Fuchs, J. A. (1983) Characterization of the mRNA coding for ribonucleoside diphosphate reductase in *Escherichia coli*. J. Bacteriol. **156**, 1192-1197

14 Stubbe, J. and Riggs-Gelasco, P. (1998) Harnessing free radicals: formation and function of the tyrosyl radical in ribonucleotide reductase. Trends Biochem. Sci. **23**, 438-443

15 Sjöberg, B. M., Reichard, P., Gräslund, A. and Ehrenberg, A. (1978) The tyrosine free radical in ribonucleotide reductase from *Escherichia coli*. J. Biol. Chem. **253**, 6863-6865

16 Atkin, C. L., Thelander, L., Reichard, P. and Lang, G. (1973) Iron and free radical in ribonucleotide reductase. Exchange of iron and Mossbauer spectroscopy of the protein B2 subunit of the *Escherichia coli* enzyme. J. Biol. Chem. **248**, 7464-7472

17 Stubbe, J., Nocera, D. G., Yee, C. S. and Chang, M. C. (2003) Radical initiation in the class I ribonucleotide reductase: long-range proton-coupled electron transfer? Chem. Rev. **103**, 2167-2201

18 Nordlund, P., Sjöberg, B. M. and Eklund, H. (1990) Three-dimensional structure of the free radical protein of ribonucleotide reductase. Nature. **345**, 593-598
19 Yokoyama, K., Smith, A. A., Corzilius, B., Griffin, R. G. and Stubbe, J. (2011) Equilibration of tyrosyl radicals (Y356•, Y731•, Y730•) in the radical propagation pathway of the *Escherichia coli* class Ia ribonucleotide reductase. J. Am. Chem. Soc. **133**, 18420-18432
20 Minnihan, E. C., Seyedsayamdost, M. R., Uhlin, U. and Stubbe, J. (2011) Kinetics of radical intermediate formation and deoxynucleotide production in 3-aminotyrosine-substituted *Escherichia coli* ribonucleotide reductases. J. Am. Chem. Soc. **133**, 9430-9440
21 Seyedsayamdost, M. R., Xie, J., Chan, C. T., Schultz, P. G. and Stubbe, J. (2007) Site-specific insertion of 3-aminotyrosine into subunit $\alpha 2$ of *E. coli* ribonucleotide reductase: direct evidence for involvement of Y730 and Y731 in radical propagation. J. Am. Chem. Soc. **129**, 15060-15071
22 Sjöberg, B. M., Karlsson, M. and Jörnvall, H. (1987) Half-site reactivity of the tyrosyl radical of ribonucleotide reductase from *Escherichia coli*. J. Biol. Chem. **262**, 9736-9743
23 Climent, I., Sjöberg, B. M. and Huang, C. Y. (1991) Carboxyl-terminal peptides as probes for *Escherichia coli* ribonucleotide reductase subunit interaction: kinetic analysis of inhibition studies. Biochemistry. **30**, 5164-5171
24 Seyedsayamdost, M. R., Yee, C. S., Reece, S. Y., Nocera, D. G. and Stubbe, J. (2006) pH Rate profiles of FnY356-R2s (n = 2, 3, 4) in *Escherichia coli* ribonucleotide reductase: evidence that Y356 is a redox-active amino acid along the radical propagation pathway. J. Am. Chem. Soc. **128**, 1562-1568
25 Climent, I., Sjöberg, B. M. and Huang, C. Y. (1992) Site-directed mutagenesis and deletion of the carboxyl terminus of *Escherichia coli* ribonucleotide reductase protein R2. Effects on catalytic activity and subunit interaction. Biochemistry. **31**, 4801-4807
26 Thelander, L. (1974) Reaction mechanism of ribonucleoside diphosphate reductase from *Escherichia coli*. Oxidation-reduction-active disulfides in the B1 subunit. J. Biol. Chem. **249**, 4858-4862
27 Brown, N. C. and Reichard, P. (1969) Role of effector binding in allosteric control of ribonucleoside diphosphate reductase. J. Mol. Biol. **46**, 39-55
28 Eriksson, M., Uhlin, U., Ramaswamy, S., Ekberg, M., Regnström, K., Sjöberg, B. M. and Eklund, H. (1997) Binding of allosteric effectors to ribonucleotide reductase protein R1: reduction of active-site cysteines promotes substrate binding. Structure. **5**, 1077-1092
29 Larsson, K. M., Jordan, A., Eliasson, R., Reichard, P., Logan, D. T. and Nordlund, P. (2004) Structural mechanism of allosteric substrate specificity regulation in a ribonucleotide reductase. Nat. Struct. Mol. Biol. **11**, 1142-1149
30 Larsson, K. M., Andersson, J., Sjöberg, B. M., Nordlund, P. and Logan, D. T. (2001) Structural basis for allosteric substrate specificity regulation in anaerobic ribonucleotide reductases. Structure. **9**, 739-750
31 Aravind, L., Wolf, Y. I. and Koonin, E. V. (2000) The ATP-cone: an evolutionarily mobile, ATP-binding regulatory domain. J. Mol. Microbiol. Biotechnol. **2**, 191-194
32 Thelander, L. (1973) Physicochemical characterization of ribonucleoside diphosphate reductase from *Escherichia coli*. J. Biol. Chem. **248**, 4591-4601
33 Brown, N. C. and Reichard, P. (1969) Ribonucleoside diphosphate reductase. Formation of active and inactive complexes of proteins B1 and B2. J. Mol. Biol. **46**, 25-38

34 Ekberg, M., Sahlin, M., Eriksson, M. and Sjöberg, B. M. (1996) Two conserved tyrosine residues in protein R1 participate in an intermolecular electron transfer in ribonucleotide reductase. J. Biol. Chem. **271**, 20655-20659
35 Rova, U., Goodtzova, K., Ingemarson, R., Behravan, G., Gräslund, A. and Thelander, L. (1995) Evidence by site-directed mutagenesis supports long-range electron transfer in mouse ribonucleotide reductase. Biochemistry. **34**, 4267-4275
36 Larsson, A. and Sjöberg, B. M. (1986) Identification of the stable free radical tyrosine residue in ribonucleotide reductase. EMBO J. **5**, 2037-2040
37 Seyedsayamdost, M. R., Chan, C. T., Mugnaini, V., Stubbe, J. and Bennati, M. (2007) PELDOR spectroscopy with DOPA- β 2 and NH2Y- α 2s: distance measurements between residues involved in the radical propagation pathway of *E. coli* ribonucleotide reductase. J. Am. Chem. Soc. **129**, 15748-15749
38 Ando, N., Brignole, E. J., Zimanyi, C. M., Funk, M. A., Yokoyama, K., Asturias, F. J., Stubbe, J. and Drennan, C. L. (2011) Structural interconversions modulate activity of *Escherichia coli* ribonucleotide reductase. Proc. Natl. Acad. Sci. U. S. A. **108**, 21046-21051
39 Rofougaran, R., Crona, M., Vodnala, M., Sjöberg, B. M. and Hofer, A. (2008) Oligomerization status directs overall activity regulation of the *Escherichia coli* class Ia ribonucleotide reductase. J. Biol. Chem. **283**, 35310-35318
40 Edwards, P. P., Gray, H. B., Lodge, M. T. and Williams, R. J. (2008) Electron transfer and electronic conduction through an intervening medium. Angew. Chem. Int. Ed. Engl. **47**, 6758-6765
41 Xu, H., Faber, C., Uchiki, T., Fairman, J. W., Racca, J. and Dealwis, C. (2006) Structures of eukaryotic ribonucleotide reductase I provide insights into dNTP regulation. Proc. Natl. Acad. Sci. U. S. A. **103**, 4022-4027
42 Fairman, J. W., Wijerathna, S. R., Ahmad, M. F., Xu, H., Nakano, R., Jha, S., Prendergast, J., Welin, R. M., Flodin, S., Roos, A., Nordlund, P., Li, Z., Walz, T. and Dealwis, C. G. (2011) Structural basis for allosteric regulation of human ribonucleotide reductase by nucleotide-induced oligomerization. Nat. Struct. Mol. Biol. **18**, 316-322
43 Kashlan, O. B. and Cooperman, B. S. (2003) Comprehensive model for allosteric regulation of mammalian ribonucleotide reductase: refinements and consequences. Biochemistry. **42**, 1696-1706
44 Reichard, P., Eliasson, R., Ingemarson, R. and Thelander, L. (2000) Cross-talk between the allosteric effector-binding sites in mouse ribonucleotide reductase. J. Biol. Chem. **275**, 33021-33026
45 Eriksson, S., Thelander, L. and Akerman, M. (1979) Allosteric regulation of calf thymus ribonucleoside diphosphate reductase. Biochemistry. **18**, 2948-2952
46 Aye, Y. and Stubbe, J. (2011) Clofarabine 5'-di and -triphosphates inhibit human ribonucleotide reductase by altering the quaternary structure of its large subunit. Proc. Natl. Acad. Sci. U. S. A. **108**, 9815-9820
47 Rofougaran, R., Vodnala, M. and Hofer, A. (2006) Enzymatically active mammalian ribonucleotide reductase exists primarily as an α 6 β 2 octamer. J. Biol. Chem. **281**, 27705-27711
48 Thelander, L., Eriksson, S. and Akerman, M. (1980) Ribonucleotide reductase from calf thymus. Separation of the enzyme into two nonidentical subunits, proteins M1 and M2. J. Biol. Chem. **255**, 7426-7432

49 Wang, J., Lohman, G. J. and Stubbe, J. (2007) Enhanced subunit interactions with gemcitabine-5'-diphosphate inhibit ribonucleotide reductases. Proc. Natl. Acad. Sci. U. S. A. **104**, 14324-14329
50 Bennati, M., Robblee, J. H., Mugnaini, V., Stubbe, J., Freed, J. H. and Borbat, P. (2005) EPR distance measurements support a model for long-range radical initiation in *E. coli* ribonucleotide reductase. J. Am. Chem. Soc. **127**, 15014-15015
51 Ge, J., Yu, G., Ator, M. A. and Stubbe, J. (2003) Pre-steady-state and steady-state kinetic analysis of *E. coli* class I ribonucleotide reductase. Biochemistry. **42**, 10071-10083
52 Erickson, H. K. (2001) Kinetics in the pre-steady state of the formation of cystines in ribonucleoside diphosphate reductase: evidence for an asymmetric complex. Biochemistry. **40**, 9631-9637

Figure legends

Figure 1. Catalytic mechanism of *E. coli* class Ia RNR. Class Ia RNRs act on all four ribonucleoside diphosphates (B = A, T, G, C). Hydrogen abstraction at the 3′ position of the substrate is initiated by the essential thiyl radical (C439). Two additional cysteines at the α_2 active site (C225, C462) act as a redox sulfhydryl pair and are directly involved in the reduction of NDPs to deoxyribonucleoside diphosphates (dNDPs). Re-reduction of the active site disulfide occurs via disulfide exchange with two cysteine residues on the C-terminal tails of the nucleotide-binding subunit, α_2. The C-terminal tail disulfide is re-reduced in a thioredoxin/thioredoxin reductase/NADPH-dependent or equivalent reaction. Kinases and additional enzymes convert the dNDP products of RNR into the direct precursors for DNA, deoxyribonucleoside triphosphates (dNTPs).

Figure 2. Structures of the class Ia *E. coli* RNR subunits. (a) Crystal structures of α_2 (generated by superposition of PDB: 4R1R, 3R1R) [28]. Monomers are colored light blue and gray with N-terminal cone domains in green. C-terminal peptides of β are colored in orange. Bound nucleotides are colored by atoms (gray carbon, blue nitrogen red oxygen, orange phosphorus). dTTP is bound in the specificity site, GDP is bound in the specificity site, and AMP-PNP is bound in the activity site. Key residues are shown in dark blue. (b) Crystal structure of β_2 (PDB: 1RIB) [18]. Monomers are colored red and orange. Flexible C-terminal tails (illustrated as dashed lines) are responsible for interacting with the α_2 subunit and contain the Y356 residue that is critical for radical propagation. Key residues are shown in dark blue with Fe atoms adjacent to Y122 colored in green.

Figure 3. Structural insight into the active complex. (a) In the proposed $\alpha_2\beta_2$ model for the active complex (shown with same coloring as in Fig. 2), the structures of the individual subunits were rigid-body docked along their symmetry axes, bringing the residues involved in radical transfer as close as possible across the subunit interface [8]. The shortest W48-Y731 distance (indicated with double arrows) in this model is 23 Å. (b) Left: The compact subunit arrangement in the proposed docking model is consistent with a low-resolution shape reconstruction of the active complex obtained by SAXS and also fits SAXS data in a global analysis [38]. The disconnected density in this reconstruction is due the presence of a small population of inhibited complexes in equilibrium with the active complex. Right: The molecular envelope shown here is the average of ten *ab initio* DAMMIF models generated from data on 6 μM RNR in the presence of the substrate CDP [38], with the contributions from a small population of inhibited complexes subtracted.

Figure 4. Crystal structure of the dATP-inhibted $\alpha_4\beta_4$ complex. The inhibited complex (PDB: 3UUS) is a ring of alternating subunits making contact at the activity site [38] (shown with same coloring as in Fig. 2). dATP is bound in both the activity and specificity sites. The C-terminal tails of β_2 (shown in orange/red) are bound in the previously determined peptide-binding sites on α_2. The shortest W48-Y731 distance is 55 Å (indicated by double arrows), much too long for radical transfer even with a bridging Y356.

Figure 5. Model for allosteric regulation of activity in *E. coli* class Ia RNR (shown with same coloring as in Fig. 2).

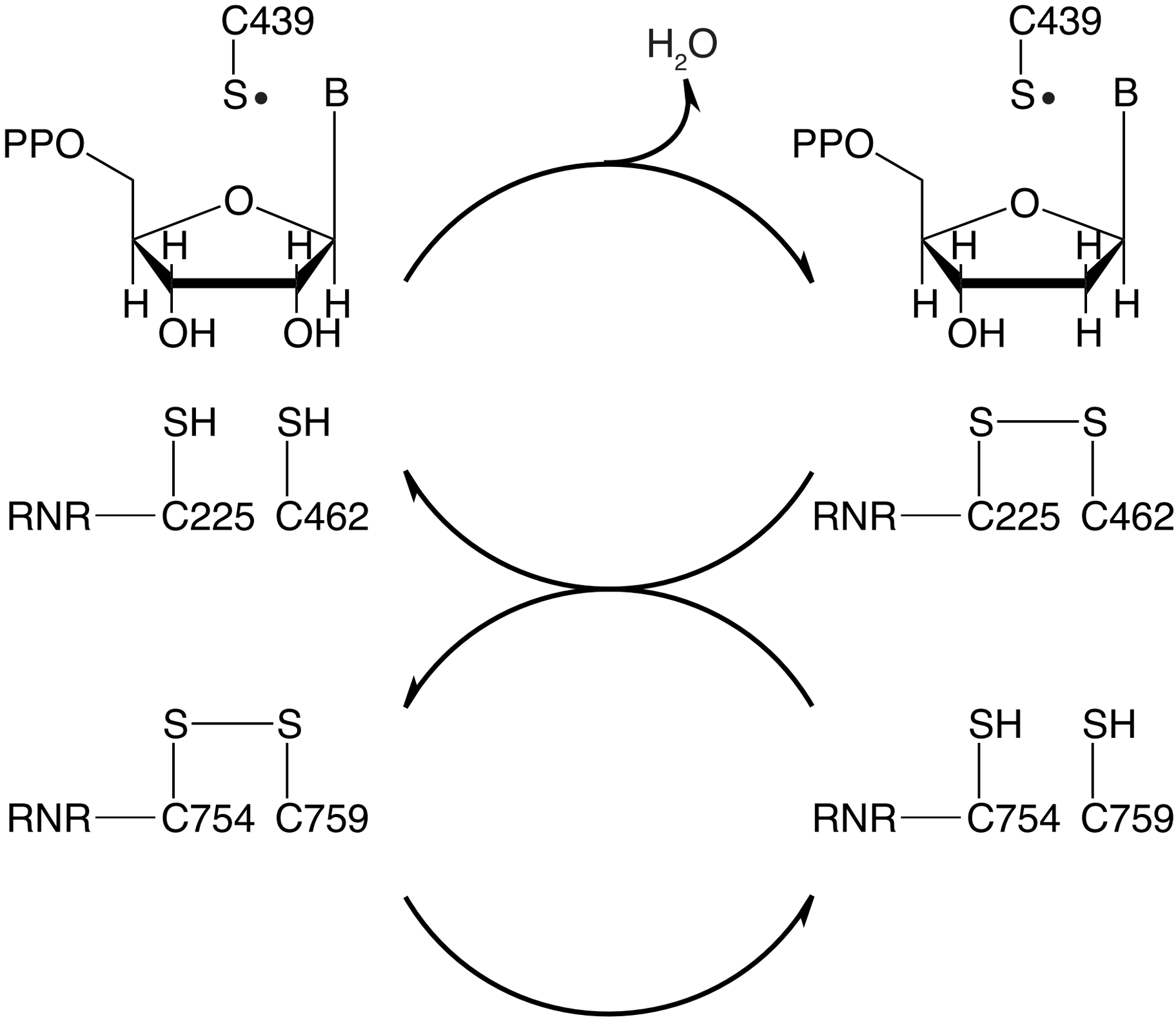
C439
S•
B
PPO
O
H
H
H
H
OH
OH
H_2O
C439
S•
B
PPO
O
H
H
H
H
OH
H
SH
SH
RNR
C225
C462
S
S
RNR
C225
C462
S
S
RNR
C754
C759
SH
SH
RNR
C754
C759
thioredoxin/
thioredoxin reductase
NADPH

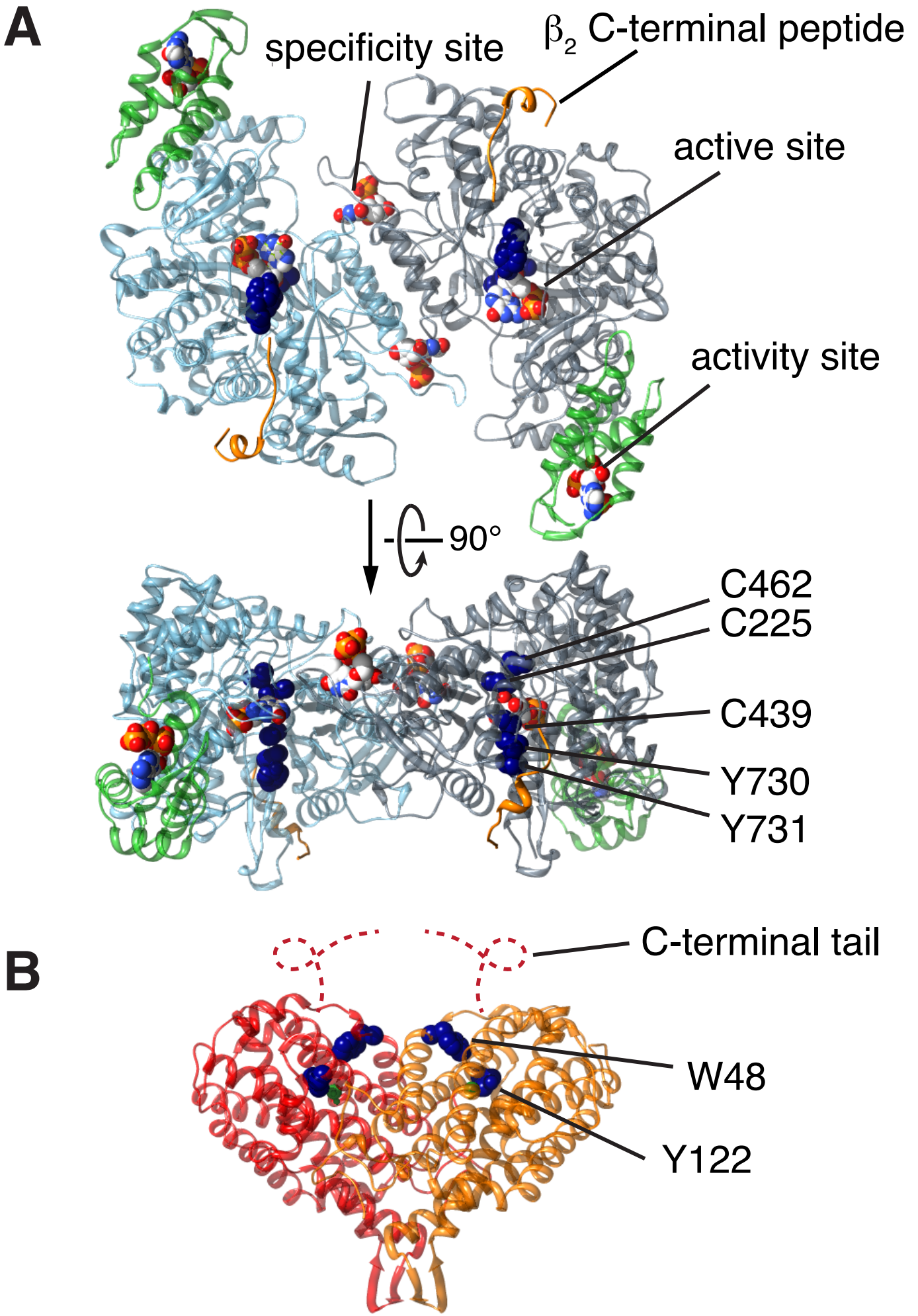
A
specificity site
β_2 C-terminal peptide
active site
activity site
90°
C462
C225
C439
Y730
Y731
B
C-terminal tail
W48
Y122

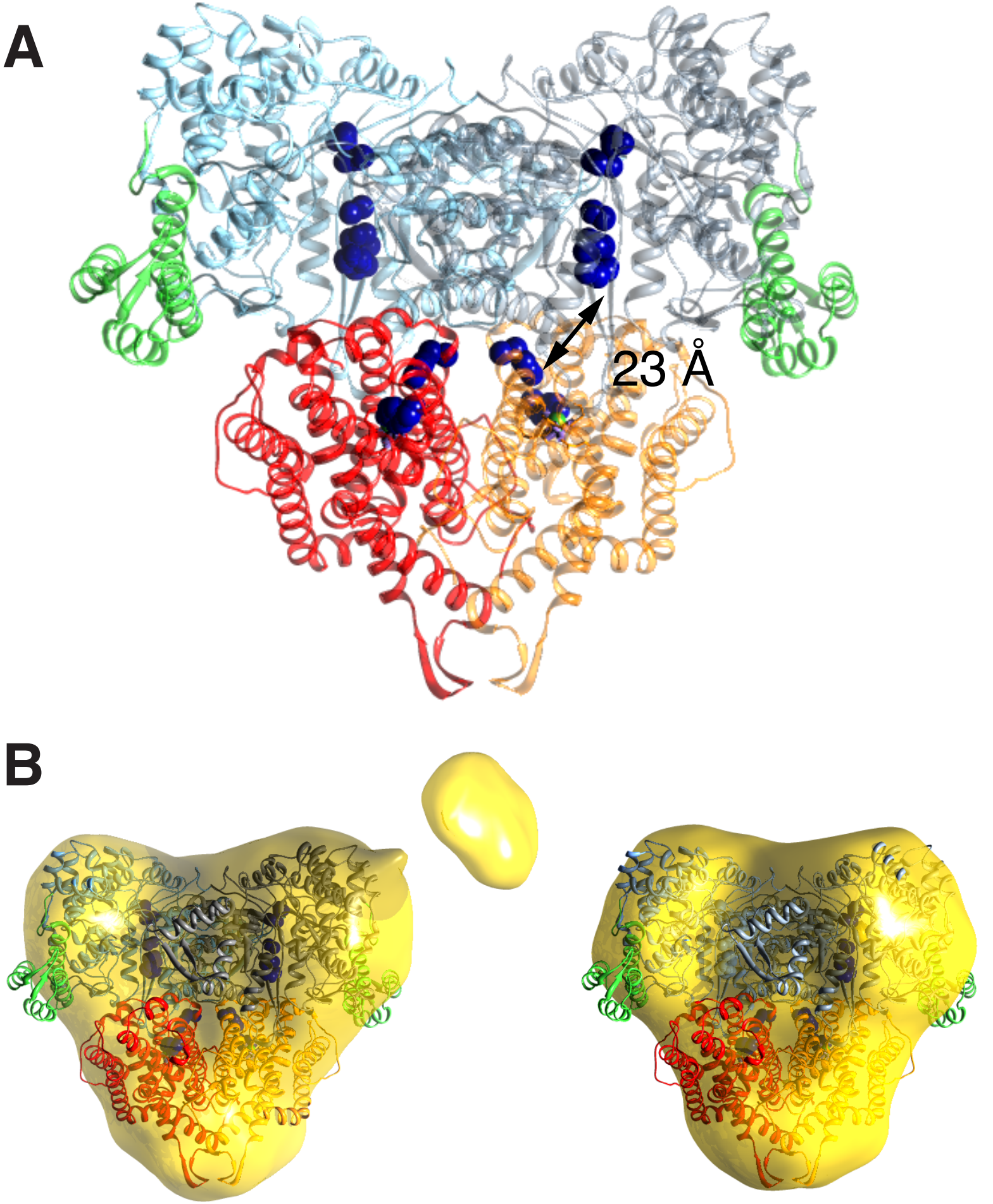
A
23 Å
B

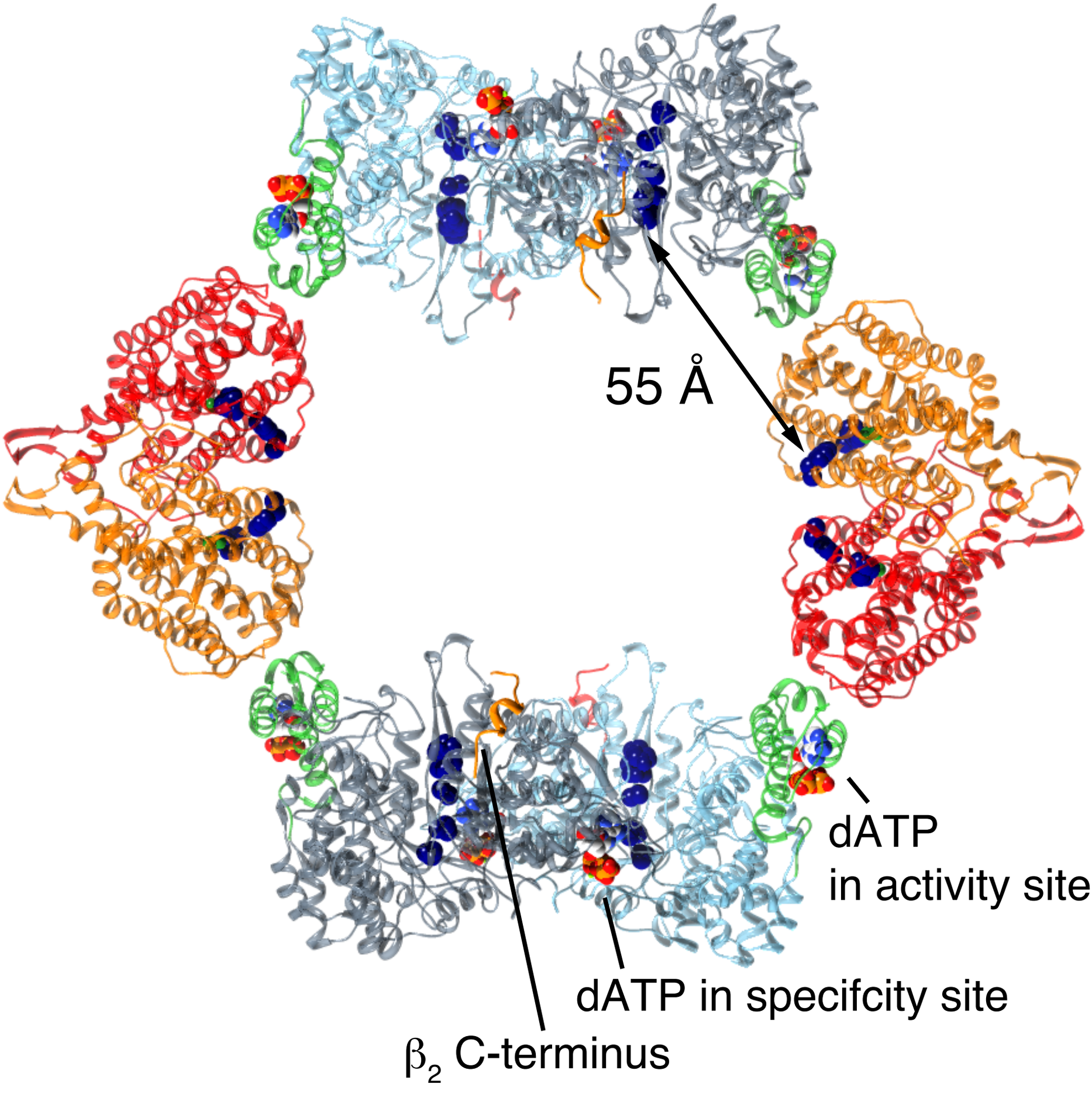
55 Å
dATP
in activity site
dATP in specifcity site
β_2 C-terminus

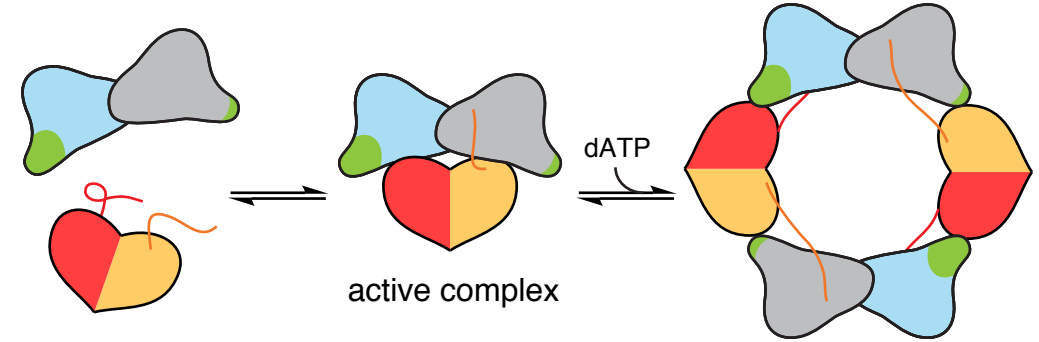
dATP
dissociated subunits
active complex
dATP-inactive complex